OLEDp1-4L
(Late-News Paper)

A Study on the Hyperfluorescence Effect of Thermally Activated Delayed Fluorescent Material Showing Aggregation Induced Emission

Eun Young Park, Vasudevan Thangaraji and Min Chul Suh*

Dept. of Information Display, Kyung Hee University, Seoul 02447, Korea
Tel.:82-2-961-0694, E-mail: mcsuh@khu.ac.kr

Keywords: Thermally activated delayed fluorescence (TADF), aggregation induced emission (AIE), concentration quenching, low roll off, Hyper fluorescence (HF), organic light emitting diode (OLED)

ABSTRACT

In this paper, the exciton behavior was analyzed using bis[4-(9,9-dimethyl-9,10-dihydroacridine)phenyl]sulfone (DMAC-DPS) composed of donor-acceptor-donor (D-A-D) units. Interestingly, DMAC-DPS showed aggregation-induced emission (AIE) characteristics. We predicted the device performances by calculating the concentration quenching rate of DMAC-DPS with AIE characteristics. In addition, triplet-triplet annihilation (TTA) and singlet-triplet annihilation (STA) were analyzed according to the doping concentration to understand the exciton behavior related to aggregation of DMAC-DPS as a sensitizer.

1 INTRODUCTION

Organic light-emitting diodes (OLEDs) have been developed for nearly 30 years because they can show many advantages when applied to displays and thin-film lighting, and recently are rapidly being put into practical use.[1-3] Meanwhile, organic light-emitting materials for OLEDs are developing from 1st generation fluorescence to 4th generation hyperfluorescence (HF), and the characteristic of HF is the use of 3rd generation TADF (Thermally Activated Delayed Fluorescence) material as a sensitizer. Most TADF materials are designed to reduce the energy gap between singlet (S_1) and triplet (T_1) by twisting the donor-acceptor (D-A) to completely separate the electron distribution into HOMO and LUMO. Therefore, a method that allows a very fast RISC (Reverse Intersystem Crossing) process due to a small energy difference between the S_1 and T_1 energy levels (ΔE_{ST}) so that they allows 100% of singlet excitons to be used. However, in the case of the D-A structure composed of a typical twisted internal charge transfer (TICT) complex, the molecular bonding strength is weakened and concentration quenching occurs at a high concentration. In addition, the spatially separated TADF structure has a wide emission spectrum, which negatively affects the color purity of OLEDs. Therefore, an appropriate doping concentration is required.

Meanwhile, to compensate for the shortcomings of TADF as aforementioned, a fourth-generation technology, HF, was developed. HF is a process in which singlet excitons of TADF sensitizer generated with the aid of TADF material transfer energy to the fluorescent dopant through the Förster Energy Transfer (FRET) process. Therefore, it is important to design a sensitizer that can transfer energy efficiently. In this paper, the concentration quenching rate was calculated according to the aggregation phenomenon of DMAC-DPS having a D-A-D structure. In addition, the device was manufactured by gradually increasing the concentration (10wt% → 80wt%), and the exciton behavior according to the aggregation phenomenon was realized by calculating the TTA (triplet-triplet annihilation) and STA (singlet-triplet annihilation) rate constants. In addition, by calculating the exciton loss rate according to the exciton density, it was confirmed how efficiently energy is transferred when these materials act as a TADF sensitizer in the HF device.

2 EXPERIMENT

As Indium tin oxide (ITO) patterned by the photolithography process has an active area of 3 x 3 mm^2. We cleaned the ITO substrates with acetone and isopropyl alcohol (IPA) for 10 min, followed by UV-ozone treatment for 15 min to increase adhesion. The PEDOT:PSS used as the HIL was spin-coated on an ITO substrate at 10,000 rpm for 22 s. The spin-coated glass was then transferred to an N_2-filled glove box and annealed at 160 °C for 20 min. Afterwards, all HTL and ETL materials were deposited at ~0.5 Å/s. Also, in the case of EML, as an experiment to confirm concentration quenching, DPEPO was doped with DMAC-DPS at 10 wt% → 80 wt%, respectively. Finally, LiF and Al were deposited at 0.3 Å/s and 2.0 Å/s, respectively. All depositions were performed under 10^{-7} Torr pressure.

In addition, the aggregation phenomenon was confirmed by measuring the photoluminescence (PL) intensity and transient PL (TRPL). The DMAC-DPS was dissolved in 5 X 10^{-5} M in tetrahydrofuran (THF) solvent according to water fractions (f_w).

3 RESULTS

In this paper, bis[2-(diphenylphosphino)phenyl] ether oxide (DPEPO) was used as the host to confirm the aggregation phenomenon, and bis[4-(9,9-dimethyl-9,10-dihydroacridine)phenyl]sulfone (DMAC-DPS) with donor-acceptor-donor (D-A-D) structure was used as the

TADF material. **Fig.1** shows the structure and energy diagrams of DPEPO and DMAC-DPS.

In order to confirm the aggregation properties of the TADF structure. We dissolved in a THF-water mixture and then measured photoluminescence (PL) spectra and transient PL (TRPL) according to the water fraction (f_w).

As shown in **Fig. 2(a)** of DMAC-DPS, when the water fraction (f_w) was increased, the PL emission wavelength was red-shifted at 40%, while PL emission rapidly blue-shifted from 50%. In addition, the result of TRPL measurement (**Fig. 2(b)**), it was confirmed that delayed lifetime rapidly increased from 50%, due to the blue-shift in the PL emission spectra. Hence, we confirmed the DMAC-DPS structure (D-A-D) having a twisted internal charge transfer (TICT) complex, so the reason for red-shifted by 40%. Meanwhile, in order to confirm the reason for the blue-shift, we optimized the molecular structure of DMAC-DPS as shown in **Fig. 2(c)**. However, from the side view of the DAMC-DPS structure is very difficult to stack. As above the results, it can be noticed that aggregation emission proceeds rapidly from 50%. In addition, the reason for the rapid increase in the delayed lifetime from 50%, it can be assumed that the non-radiative path is blocked and as well π-π stacking is suppressed. Hence, DMAC-DPS having aggregation-induced emission (AIE) properties.

Furthermore, we calculated the concentration quenching rate (k_{CQ}) using a three-level model to understand the physical behavior of DMAC-DPS with AIE characteristics.[4] The photophysical properties were calculated and the values are shown in **Table 1**. The TRPL was measured according to increasing the doping concentration of DMAC-DPS with the host (DPEPO) from 10 wt% → 80 wt%. The TRPL spectra are shown in **Fig.3(a)**, it was not any significant changes in the time-delay spectra of DMAC-DPS according to increasing the doping concentration. These results are different from the previously reported concentration quenching phenomenon.[4] Because this material is a strong AIE tendency, so the concentration quenching phenomenon was not followed. In addition, the k_{CQ} rate of DMAC-DPS was very low, about ~10^4 s^{-1}. Therefore, the concentration quenching is not affected in the DMAC-DPS material, according to the doping concentration. It was expected from **Fig. 3(c)** and **3(d)**, so it's possible to fabricate relatively high dopant concentration devices. To confirm this phenomenon from the theoretical calculations, we design the following device structure. The energy diagram of the device is shown in **Fig. 4(a)**.

Device A : ITO / PEDOT: PSS (40 nm) / TAPC (20 nm) / mCP (10 nm) / DPEPO: DMAC-DPS (30 nm, x wt%) (x = 10, 20, 40, 60, 80) / TSPO1 (5 nm) / TPBI (30 nm) / LiF (1 nm) / Al (100 nm)

The EL performance of **Device A** was shown in **Fig. (4)** and **Table 2**. The turn-on voltage (V_{on}) of **Device A** was measured at 5.0 (10 wt%), 4.0 (20 wt%), 3.0 (40 wt%), 3.5 (60 wt%), and 2.5 V (80 wt%). In addition, the operating voltage (V_{op}) was measured at 8.0 (10 wt%), 9.5 (20 wt%), 6.0 (40 wt%), 5.5 (60 wt%), and 5.0 V (80 wt%). The maximum current efficiency (CE) of **Device A** were 22.3 (10 wt%), 29.0 (20 wt%), 31.8 (40 wt%), 34.2 (60 wt%), and 26.9 cd/A (80 wt%). In **Fig. 4(c)** DMAC-DPS with AIE properties showed the highest efficiency of 34.2 cd/A at 60 wt%, therefore we confirmed relatively high doping concentration was possible. This trend is related to the previously calculated k_{CQ} rate. Hence, the DMAC-DPS with AIE properties was not significant in the effect of the exciton quenching according to the doping concentration.

In order to analyze the device characteristics according to the dopant concentration for more detail, we calculated triplet-triplet annihilation (TTA) and singlet-triplet annihilation (STA) were using the following equations:[5]

$$\frac{\mathrm{EQE}}{\mathrm{EQE}_0} = \frac{J_{1/2}}{4J}\left(\sqrt{1+8\frac{J}{J_{1/2}}}-1\right) \qquad (1)$$

where $J_{1/2}$ is the current density at $\mathrm{EQE} = \mathrm{EQE}_0/2$ and EQE_0 means EQE without TTA effects. TTA and STA values were calculated through the fitting results, it can be seen in **Fig. 5(a)** and **Table 3**.

As a result of the above calculation, the DMAC-DPS of k_{TTA} values were increased from 8.55 × 10^{-13} cm^3/s to 5.92 × 10^{-12} cm^3/s when the doping concentration is increased from 10wt% →80wt%, while, k_{STA} values were increased from 5.84 × 10^{-11} cm^3/s to 1.78 × 10^{-10} cm^3/s. Therefore, k_{TTA} and k_{STA} values were increased by 6.9 and 3.0 times, respectively, it means there is no significant changes according to the doping concentration (**Fig. 5a**). Furthermore, exciton behavior was analyzed according to the doping concentration by applying TTA and STA fitting to calculate the exciton density and exciton loss (**Fig. 5b**). As a result of the above calculation, there was no significant change in exciton loss according to doping concentration. The k_{TTA} and k_{STA} values are increased meanwhile not affect the exciton loss according to the doping concentration. Hence, the DMAC-DPS device shows low roll-off. These results and previously calculated k_{CQ} rate values are supported by the device performance.

Further, we fabricate an HF device to verify the energy transfer process at higher concentrations. The energy diagram of the device can be seen in **Fig. 6(a)**.

Device B : ITO / PEDOT: PSS (40 nm) / TAPC (20 nm) / mCP (10 nm) / DPEPO: DMAC-DPS: TBPe (30 nm, 60 wt%, 1 wt%) / TSPO1 (5 nm) / TPBI (30 nm) / LiF (1 nm) / Al (100 nm)

Fig. 6(b) shows the *J-V-L* curves of **Device B**, the V_{on} was measured 3.0 V and the V_{op} was measured 5.5 V. The maximum CE of **Device B** was 28.1 cd/A (**Fig. 6(c)** and **Table 4**). DMAC-DPS with AIE characteristics are showed high efficiency with higher dopant concentration. Moreover, further understanding of the FRET energy transfer process, we calculated the FRET radius by the equation (2).[6]

$$k_{FRET} = (1/\tau_D)(R_F/R)^6 \qquad (2)$$

The τ_D is the radiative decay lifetime (TADF) and R_F is the FRET radius, and R is the average distance (TADF and the fluorescence dopant). R_F and R values were obtained from Eq(2) and the values were 2.36 nm and 2.18 nm, respectively. The calculated k_{FRET} is 4.38 × 10^7 s^{-1}. The R_F value is greater than R-value, so we can confirm that FRET and DET occurred effectively.

4 CONCLUSIONS

In summary, the exciton behavior of DMAC-DPS with AIE properties was analyzed. As a result, the DMAC-DPS with AIE characteristics maintained high efficiency of 34.2 cd/A at 60wt%. However, this device shows low roll-off characteristics according to doping concentration as a result of TTA and STA fitting. In addition, FRET occurred effectively in the hyperfluorescence device despite the relatively high concentration. This device performance is different from the concentration quenching phenomenon of the conventional TADF materials.

ACKNOWLEDGMENT

This work was supported by Basic Science Research Program through the National Research Foundation of Korea (NRF) funded by the Ministry of Education (2021R1A2C1008725). This work was also supported by the Industrial Strategic Technology Development Program (20011059) funded by MOTIE, Korea.

REFERENCES

[1] C. W. Tang, and S. A VanSlyke., Organic electroluminescent diodes. Appl. Phys. Lett. Vol. 51, pp. 913−6 (1987).

[2] H. S Nalwa. L. S. Rohwer., Handbook of Luminescence, Display Materials and Devices, American Scientific Publishers USA April 6, 2003.

[3] M. Choi, Y. J. Park., B. K. Sharma, S. R. Bae, S. Y. Kim, J. H. Ahn., Flexible active-matrix organic light-emitting diode display enabled by MoS2 thin-film transistor. Sci. Adv. Vol. 4, pp. 8721-8 (2018).

[4] H. S. Kim, S. R. Park, M. C. Suh., Concentration Quenching Behavior of Thermally Activated Delayed Fluorescence in a Solid Film. J. Phys. Chem. C. Vol. 121, pp. 13986-13997 (2017).

[5] M. A. Baldo, C. Adachi, S. R. Forrest., Transient Analysis of Organic Electro Phosphorescence. Phys. Rev. B: Condens. Matter Mater. Phys. Vol. 62, pp. 10967 (2000).

[6] T. Forster., 10th Spiers Memorial Lecture. Transfer Mechanisms of Electronic Excitation. Discuss. Faraday Soc. Vol. 27, pp. 7−17 (1959).

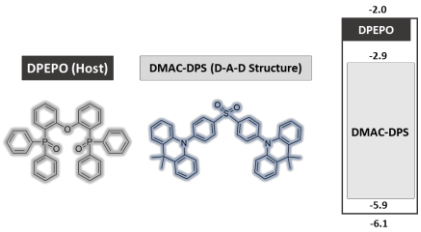

Fig. 1 Molecular structure DPEPO (host), DMAC-DPS (D-A structure) and energy band diagram.

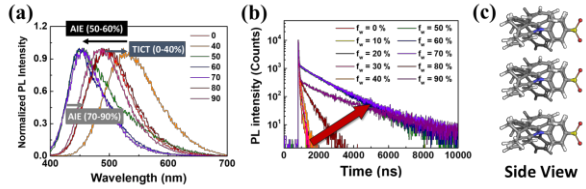

Fig. 2 (a) PL spectra according to f_w (b) TRPL decay lifetime according to f_w (c) Optimized structure of side view.

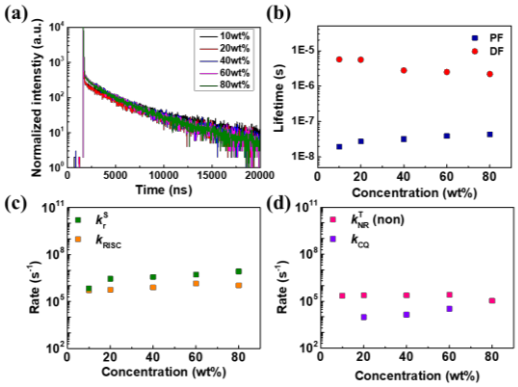

Fig. 3 (a)TRPL decay according to doping concentration (b) Prompt and delayed lifetime (c) Photo-physical properties of DMAC-DPS (d) k_{NR}^{T} and k_{CQ} according to doping concentration.

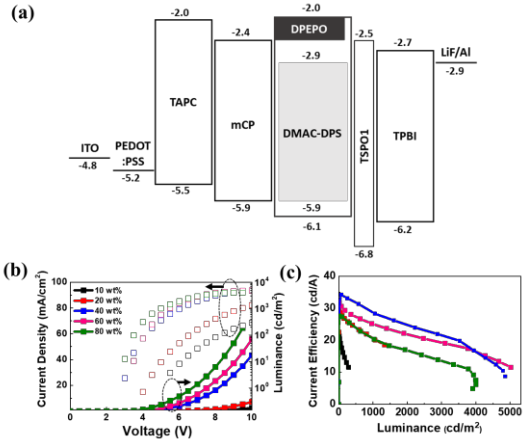

Fig. 4 (a) Device configuration of **Device A** (b) *J-V-L* (c) Current efficiency of **Device A**.

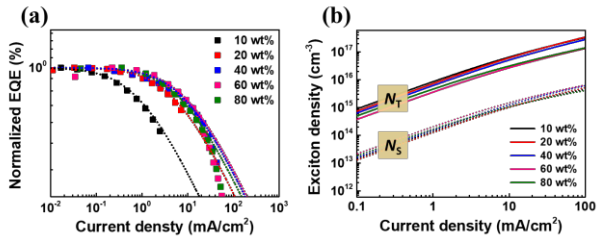

Fig. 5 (a) Normalized EQE according to current density of **Device A** (fitting line is expressed as a dash line) (b) exciton density N_S and N_T of **Device A**

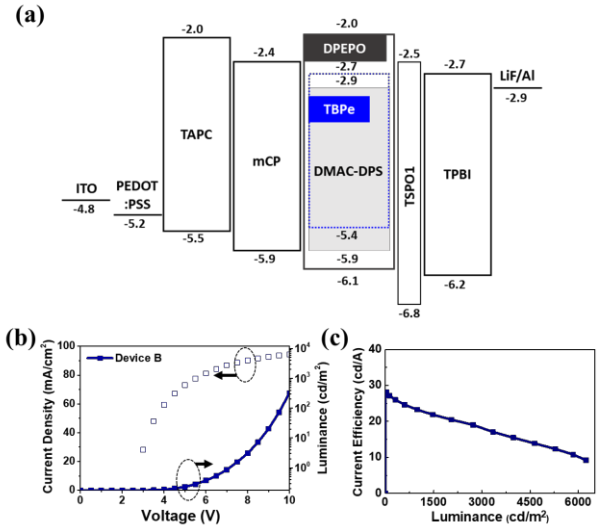

Fig. 6 (a) Device configuration of **Device B** (b) *J-V-L* (c) Current efficiency of **Device B**.

Table 1. Photophysical properties of DMAC-DPS.

DMAC-DPS	k_r^S (10^6 s^{-1})	k_{RISC} (10^5 s^{-1})	k_{nr}^T (10^5 s^{-1})	k_{CQ} (10^4 s^{-1})
10wt%	0.68	5.38	2.23	-
20wt%	2.82	5.71	2.33	1.0
40wt%	3.70	7.86	2.37	1.4
60wt%	5.25	14.0	2.56	3.3
80wt%	8.44	11.0	1.06	-

Table 2. Device characteristics of **Device A** according to concentration change (CE: current efficiency)

Device A	V_{on}[a]/V_{op}[b,c]	CE (%) Max / 1000 cd/m²	CIE (x,y)[b,c]
10wt%	5.5/8.0[c]	22.3/17.6[c]	(0.16,0.25)
20wt%	4.0/9.5	29.0/20.1	(0.16,0.24)
40wt%	3.0/6.0	31.8/25.2	(0.16,0.27)
60wt%	3.5/5.5	34.2/28.3	(0.16,0.29)
80wt%	2.5/5.0	27.6/20.3	(0.16,0.29)

[a]Measured at 1 cd/m². [b]Measured at 1000 cd/m². [c]Measured at 100 cd/m².

Table 3. TTA and STA values for **Device A**

Device A	k_{TTA} (cm^3/s)	k_{STA} (cm^3/s)
10wt%	8.55 X 10^{-13}	5.84 X 10^{-11}
20wt%	6.60 X 10^{-13}	4.30 X 10^{-11}
40wt%	1.06 X 10^{-12}	4.66 X 10^{-11}
60wt%	5.56 X 10^{-12}	1.07 X 10^{-10}
80wt%	5.92 X 10^{-12}	1.78 X 10^{-10}

Table 4. Device characteristics of **Device B** in HF device (CE: current efficiency)

Device	V_{on}[a]/V_{op}[b]	CE (%) Max / 1000 cd/m²	CIE (x,y)[b]
Device B	3.0/5.5	28.1/23.3	(0.14,0.24)

[a]Measured at 1 cd/m². [b]Measured at 1000 cd/m².